Optimal impedance of a lined plane surface with inviscid sheared grazing flow

Lucas Araujo Bonomo[a,b,*], André Mateus Netto Spillere[a,1], Julio Apolinário Cordioli[a], Edward James Brambley[b,c]

[a] *Department of Mechanical Engineering, Federal University of Santa Catarina, Florianopolis, 88040-900, SC, Brazil*
[b] *Mathematics Institute, University of Warwick, Coventry, CV4 7AL, United Kingdom*
[c] *WMG, University of Warwick, Coventry, CV4 7AL, United Kingdom*

Abstract

The presence of sheared grazing flow changes the acoustic absorption of a lined surface. Since acoustic waves are refracted through the boundary layer between the lined surface and the mean flow, the reflection and absorption coefficients are modified by the presence of the boundary layer, and therefore so too is the optimal impedance of the surface. A common simplification is to assume a uniform flow and take into account the refraction in the impedance boundary condition. However, there is still debate in the academic community about what is the appropriate boundary condition. We investigate the optimal impedance of a lined plane surface with an inviscid sheared flow. Optimal impedances are found both using numerical solutions to the Pridmore-Brown equation, which is the exact solution for a sheared parallel flow, and using the convected Helmholtz equation, that assumes a uniform flow, together with different boundary conditions that attempt to model the boundary layer. Results suggest that, for frequencies and Mach number typically found in turbofan aero-engines, boundary layer effects are of great importance at particular angles of incidence. We find the first order asymptotic boundary condition of Brambley (2011)[1] reproduces the same optimal impedance as the Pridmore-Brown equation in most cases. The impact of the velocity profile shape is also investigated, and results suggest the same optimal impedance is expected irrespective of the velocity profile provided the boundary layer displacement thickness is the same.

Keywords: acoustic liners, optimal impedance, impedance boundary conditions

1. Introduction

The optimal impedance in flow ducts has drawn attention from researchers because high absorption rates are often desired in this kind of application to maximize sound attenuation. This becomes particularly important in aircraft engines due to weight restrictions and aerodynamic reasons; therefore, the available lined length is kept to a minimum. Of course, liner impedance optimization is a complex task due to the multi-modal nature of the acoustic field in turbo fan engines, such that different definitions of optimal impedance are possible. For instance, we could consider the optimal liner that maximizes the in-duct sound power transmission loss.

An additional challenge in the modeling of acoustic liners is the presence of a small boundary layer between the lined surface and the free-stream steady flow. A common procedure is to solve the convected Helmholtz equation, which implicitly assumes a slip condition at the lined wall, and include any boundary layer effects into an effective impedance. In this case, continuity of pressure and normal acoustic displacement

*Corresponding author.
Email addresses: lucas.bonomo@lva.ufsc.br (Lucas Araujo Bonomo), julio.cordioli@ufsc.br (Julio Apolinário Cordioli), E.J.Brambley@warwick.ac.uk (Edward James Brambley)
[1] Currently at Dynamox S.A., Florianópolis, Brazil.

through the boundary layer is the correct assumption, as proven by Eversman and Beckemeyer [2]. The special case of an infinitely thin boundary layer is known as the Ingard–Myers boundary condition [3, 4], which is the standard choice of boundary condition in flow acoustics due to its simplified mathematical formulation. However, recent reports have indicated that predictions using the Ingard–Myers boundary condition may be inaccurate at conditions typically found in turbofan aero-engines [5]. A better description of the boundary layer physics can be obtained by retaining the first [1] and second [6] order boundary layer correction terms in the matching of pressure and acoustic displacement.

Although there are studies of the impact of the boundary layer and its simplification as boundary conditions on sound absorption [e.g. 5, 7], there are no reports on their effect on the optimal impedance of a flat surface. This is in contrast with the in-duct optimal impedance, which has been a research subject for several decades [8–12]. For the optimal impedance problem in ducts, the setup is constrained by the duct geometry, Mach number and velocity profile, which dictates the wavenumber that will require a certain optimal impedance. On the other hand, for a flat plane surface, whilst again defined by the Mach number and velocity profile, the problem allows a continuum of acoustic angles of incidences and angles of propagation with respect to the mean flow. Whilst at present the main application of liners is still within a duct, particularly in the aeronautical industry, noise regulations are becoming more stringent, and novel technologies will be necessary to achieve the target levels of noise emissions. As an example, current studies include the use of acoustic absorbing surfaces at the wing trailing edge to reduce jet noise [13–16]. Little is known about the effect of boundary layers on the optimal impedance of locally-reacting acoustic liners or, in other words, which impedances lead to maximum absorption of acoustic waves. In this work, we investigate the boundary layer effects on the optimal impedance of locally reacting flat lined surfaces. We follow the test cases of the benchmark study proposed by Gabard [5], who studied the effect of boundary conditions on acoustic absorption. A definition of optimal impedance for a plane surface is also proposed. A reference solution based on the Pridmore-Brown equation [17] is compared to the predicted optimal impedances using the Ingard–Myers [3, 4] and Brambley [1] boundary conditions. Different velocity profiles are considered, to investigate the impact of the profile shape on the optimal impedance. Finally, the error associated with incorrect predictions is evaluated in terms of the absorption coefficient.

This work is structured as follows. Section 2 presents the problem formulation, including the governing equations and the boundary conditions. Section 3 presents the definition of optimal impedance considered in this work. Section 4 presents the test cases and the main results with discussions. Finally, the conclusions are summarized in Section 5.

2. Governing Equations

In this work, normalized variables are used for convenience. Dimensional parameters are denoted by the superscript *. Distances are normalized by a reference length L^*, velocities by the speed of sound c_0^*, density by the air specific density ρ_0^*, time by L^*/c_0^*, pressure by $\rho_0^* {c_0^*}^2$ and acoustic impedance by $\rho_0^* c_0^*$. The Mach number $M \equiv U_\infty^*/c_0^*$ is defined as the ratio between the free-stream fluid velocity U_∞^* and the speed of sound. The unitary vectors for the Cartesian coordinate system are represented by $(\mathbf{e_x}, \mathbf{e_y}, \mathbf{e_z})$.

We consider the situation shown schematically in Figure 1. A small perturbation to an otherwise steady flow is given by

$$\hat{p} = p_0 + \mathrm{Re}\Big(p(y)\exp\{\mathrm{i}\omega t - \mathrm{i}k_x x - \mathrm{i}k_z z\}\Big), \tag{1a}$$

$$\hat{\mathbf{u}} = U(y)\mathbf{e_x} + \mathrm{Re}\Big(\mathbf{u}(y)\exp\{\mathrm{i}\omega t - \mathrm{i}k_x x - \mathrm{i}k_z z\}\Big), \tag{1b}$$

where $\hat{p}$ is the total pressure, $\hat{\mathbf{u}}$ is the total velocity, ω is the angular frequency, and k_x and k_z are the wavenumbers in the x- and z-directions. A locally reacting wall with impedance $Z = p/(\mathbf{u}\cdot\mathbf{n})$ is located at $y = 0$, where $\mathbf{n} = -\mathbf{e_y}$ is the unit normal pointing into the wall. Above this wall, a steady subsonic flow of velocity profile $U(y)$ is present in the positive x-direction with a thin boundary layer of thickness δ, such that $U(\delta) = M$ and $U(0) = 0$.

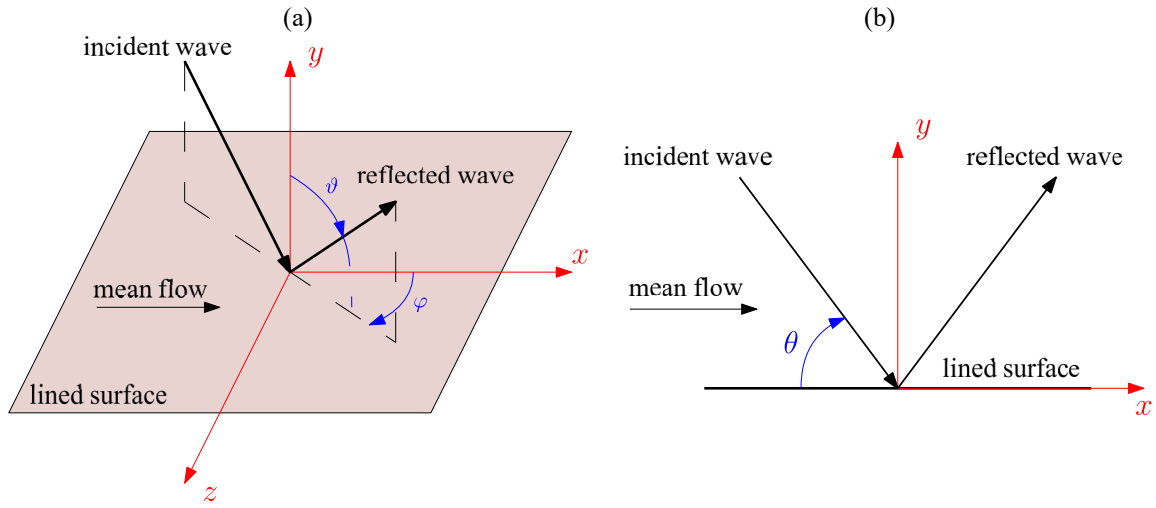

Figure 1: Sketch of the locally-reacting lined plane surface. (a) Three-dimensional case; and (b) two-dimensional case. Adapted from Gabard [5].

By neglecting viscosity and heat transfer, and assuming constant background density, the acoustic propagation in the boundary layer can be described by the Pridmore-Brown Equation (PBE) [17],

$$\begin{gathered}\frac{\mathrm{d}^2 p}{\mathrm{d}y^2} + \frac{2k_x}{\omega - Uk_x}\frac{\mathrm{d}U}{\mathrm{d}y}\frac{\mathrm{d}p}{\mathrm{d}y} + \Big((\omega - Uk_x)^2 - k_x^2 - k_z^2\Big)p = 0, \\ \text{with} \qquad \mathbf{u}\cdot\mathbf{e_y} = u_y = \frac{\mathrm{i}}{\omega - Uk_x}\frac{\partial p}{\partial y}.\end{gathered} \tag{2}$$

Outside the boundary layer, the PBE reduces to the Convected Helmholtz Equation (CHE) [18, [p. 701],

$$\nabla^2 p - \frac{\mathrm{D}_0^2 p}{\mathrm{D}t^2} = \frac{\mathrm{d}^2 p}{\mathrm{d}y^2} + \Big((\omega - Uk_x)^2 - k_x^2 - k_z^2\Big)\,p = 0, \qquad u_y = \frac{\mathrm{i}}{\omega - Mk_x}\frac{\partial p}{\partial y}. \tag{3}$$

As depicted in Figure 1, we consider a plane wave of unitary amplitude, frequency ω and angle of incidence (ϑ, φ) in 3D and θ in 2D, which is reflected with amplitude R. Downstream propagation is denoted in the three-dimensional case by $\varphi < 90°$ and in the two-dimensional case by $\theta < 90°$, and conversely for upstream propagation. In the 3D case, $k_x \equiv K\sin\vartheta\cos\varphi$ and $k_z \equiv K\sin\vartheta\sin\varphi$, where $K \equiv \omega/D$ and $D \equiv 1 + M\sin\vartheta\cos\varphi$ is the Doppler factor. In the case of two-dimensional propagation, we have $\varphi = 0$, and so $k_z = 0$. By convention [5, e.g.], the angle θ is measured relative to the surface instead of the normal as in the case of ϑ. The reader must pay attention to this angle definition, which is slightly different from typical textbook notation and was chosen to follow the literature of the field. Since θ and ϑ are complementary, the trigonometric relations $\sin\vartheta$ and $\cos\vartheta$ are replaced by $\cos\theta$ and $\sin\theta$, respectively. Therefore, the Doppler effect factor becomes $D = 1 + \cos\theta$.

The solution of the CHE in the uniform flow region is given by the sum of incident and reflected plane waves,

$$p(y) = \exp(\mathrm{i}k_y y) + R\exp(-\mathrm{i}k_y y), \tag{4}$$

where $k_y = K\cos\vartheta$. The reflected wave amplitude R depends on the boundary condition. We introduce the formulation due to Gabard [5],

$$R = \frac{Z(D\cos\vartheta + \mathrm{i}T_1) - 1 + \mathrm{i}T_0}{Z(D\cos\vartheta - \mathrm{i}T_1) + 1 + \mathrm{i}T_0}, \tag{5}$$

where T_0 and T_1 are parameters which depend on the assumed boundary condition, as discussed in Section 2.1 below. Finally, the absorption coefficient α is defined as the ratio between absorbed and incident acoustic

intensity, where the acoustic flux is given by $I_y = \frac{1}{2}(\overline{p}u_y + p\overline{u}_y)$, where an overline denotes the complex conjugate. In terms of the reflection coefficient, $\alpha = 1 - |R|^2$.

2.1. Boundary Conditions for the CHE

The standard choice in flow acoustics is the boundary condition derived by Ingard [3] and later generalized by Myers [4], hence referred as the Ingard–Myers boundary condition. It assumes continuity of pressure and normal acoustic displacement across a vanishing boundary layer. For plane surfaces, the Ingard–Myers boundary condition can be written as

$$\mathrm{i}\omega Z(\mathbf{u}\cdot\mathbf{n}) = \mathrm{i}(\omega - Mk_x)p. \tag{6}$$

It can be shown that this boundary condition leads to taking $T_0 = T_1 = 0$ in Eq. (5). In the absence of flow, this reduces to the standard definition of the reflection coefficient commonly found in acoustic textbooks [e.g. 18, p. 262].

In order to include some effects of the boundary layer, Brambley [1] performed a matched asymptotic expansion in the boundary layer region, similarly to Eversman and Beckemeyer [2]. The mean flow $U(y)$ was assumed to vary only within a small region of width $O(\delta)$ close to the wall, and the PBE (2) was solved asymptotically within this region. This inner solution was matched to the CHE solution in the uniform flow outside the boundary layer by means of matched asymptotic expansions. In effect, the inner asymptotic region could be formulated as a boundary condition to be applied to the outer CHE. Retaining only leading order terms in the inner region was shown to reproduce the Ingard–Myers boundary condition above, whilst retaining leading and first order terms resulted in an $O(\delta)$ modification to the boundary condition that incorporated the effects of the finite-thickness boundary layer (for full details, please see [1]). For a plane surface, this can be written as

$$(\mathbf{u}\cdot\mathbf{n})\left(\mathrm{i}\omega Z + (\omega - Mk_x)^2\delta I_0\right) = \left(\mathrm{i}(\omega - Mk_x) - Z\frac{\omega k_x^2 \delta I_1}{\omega - Mk_x}\right)p, \tag{7}$$

with δI_0 and δI_1 being the $O(\delta)$ modifications to the Ingard–Myers boundary condition, defined as

$$\delta I_0 = \int_0^\delta \chi_0(y)\mathrm{d}y, \qquad \delta I_1 = \int_0^\delta \chi_1(y)\mathrm{d}y, \tag{8a}$$

where

$$\chi_0(y) = 1 - \frac{(\omega - U(y)k_x)^2}{(\omega - Mk_x)^2}, \qquad \chi_1(y) = 1 - \frac{(\omega - Mk_x)^2}{(\omega - U(y)k_x)^2}. \tag{8b}$$

Taking the limit $\delta \to 0$ reduces this to the Ingard–Myers boundary condition (Eq. (6)). The reflection coefficient is again given by Eq. (5), with now

$$T_0 = -K\delta I_0 \cos\vartheta \qquad \text{and} \qquad T_1 = -K\delta I_1 D\sin^2\vartheta. \tag{9}$$

Khamis and Brambley [6] went further and again used matched asymptotic expansions to derive a boundary condition accurate to second order ($O(\delta^2)$) in the boundary layer thickness. This new solution showed increased accuracy when compared with both the Ingard–Myers boundary condition and Brambley first order correction provided the boundary layer was thin compared with a wavelength. Khamis and Brambley [19] presented the second order boundary condition for the flat Cartesian geometry used here, finding that the T_0 and T_1 parameters in the reflection coefficient (Eq. (5)) are given by

$$T_0 = -\cos\vartheta K\delta I_0 + \mathrm{i}(K_\perp^2(\delta I_0\delta I_1 + \delta^2 I_{11} - \delta^2 I_{01}) - (K^2 - K_\perp^2)\delta^2 I_2), \tag{10a}$$

$$T_1 = -\frac{DK_\perp^2\delta I_1}{K} + \mathrm{i}D\cos\vartheta((K^2 - K_\perp^2)\delta^2 I_{00} - K_\perp^2(\delta I_0\delta I_1 + \delta^2 I_3 - \delta^2 I_{10})), \tag{10b}$$

where $K_\perp^2 = k_x^2 + k_z^2$ and the higher order terms are defined as

$$\delta^2 I_2 = \int_0^\delta y\chi_0(y)\mathrm{d}y, \qquad \delta^2 I_3 = \int_0^\delta y\chi_1(y)\mathrm{d}y, \tag{11a}$$

$$\delta^2 I_{01} = \int_0^\delta \chi_0 \int_0^y \chi_1(\hat{y})\mathrm{d}\hat{y}\mathrm{d}y, \qquad \delta^2 I_{10} = \int_0^\delta \chi_1 \int_0^y \chi_0(\hat{y})\mathrm{d}\hat{y}\mathrm{d}y, \tag{11b}$$

$$\delta^2 I_{00} = \int_0^\delta \left(\int_0^y \chi_0(\hat{y})\mathrm{d}\hat{y} - \delta I_0 \right) \mathrm{d}y, \qquad \delta^2 I_{11} = \int_0^\delta \left(\int_0^y \chi_1(\hat{y})\mathrm{d}\hat{y} - \delta I_1 \right) \mathrm{d}y. \tag{11c}$$

2.2. Reflection Coefficient for the PBE

In the case of the PBE, a numerical solution of Eq. (2) is necessary, which is then matched in the far field to an incoming and outgoing plane wave in order to determine the reflection coefficient. The matching is simplified because, in the uniform flow region $y > \delta$, the PBE and the CHE are identical, and so the solution to the PBE will be of the form of Eq. (4). Hence, for any $y > \delta$, we have

$$R = \frac{1}{2\mathrm{i}k_y}\left(\mathrm{i}k_y p(y_N) - \frac{\partial p}{\partial y}(y_N)\right)\exp(\mathrm{i}k_y y_N), \tag{12}$$

with y_N the boundary of the domain governed by the PBE. In order to obtain the pressure and its derivative at $y = y_N$, the PBE is solved numerically at $N + 1$ collocation points y_i using a pseudo-spectral method, subject to boundary conditions of a unit amplitude incident wave,

$$\frac{\partial p}{\partial y} + \mathrm{i}k_y p = 2\mathrm{i}k_y \exp(\mathrm{i}k_y y_N) \quad \text{at} \quad y = y_N, \tag{13}$$

and the impedance boundary condition

$$\frac{\partial p}{\partial y} - \frac{\mathrm{i}\omega}{Z} p = 0 \quad \text{at} \quad y = 0. \tag{14}$$

The collocation points are here chosen to follow a Gauss–Lobatto distribution, and Chebyshev polynomials are used as basis functions to estimate spatial derivatives [20, p. 570]. Therefore, the computational grid is given by

$$y_i = \cos\left(\frac{\pi i}{N}\right), \quad i = 0, \ldots, N, \tag{15}$$

with N the number of points. In this work, $N = 500$ ensures convergence for all considered cases. One may obtain the differentiation matrix from

$$\mathbf{D}_{ij} = \begin{cases} \dfrac{2N^2+1}{6}, & \text{when } i = j = 0, \\ -\dfrac{2N^2+1}{6}, & \text{when } i = j = N, \\ -\dfrac{y_j}{2(1-y_j^2)}, & \text{when } i = j, 1 < j < N-1, \\ \dfrac{c_i(-1)^{i+j}}{c_j(x_i - x_j)}, & \text{when } i \neq j, \end{cases} \tag{16}$$

where $c_0 = c_N = 2$ and $c_i = 1$ otherwise. The computational domain $\xi \in [-1, 1]$ is mapped into the physical domain $y \in [0, y_N]$ by

$$y = \frac{y_N}{2}(\xi + 1) \quad \text{and} \quad \frac{\mathrm{d}}{\mathrm{d}y} = \frac{2}{y_N}\frac{\mathrm{d}}{\mathrm{d}\xi}. \tag{17}$$

In this way, a linear system of equations of the form $\mathbf{Ax} = \mathbf{b}$ is obtained, with each row imposing the discretized PBE be satisfied at one of the collocation points. This linear system is solved using the LAPACK library routine ZGESV [21, p.237]. The result is then used to find the reflection coefficient R using Eq. (12).

3. Optimal Impedance

For a given angle of incidence, perfect acoustic absorption is achieved if $|R| = 0$. For the CHE, where reflection coefficient R is simply given by Eq. (5), the optimal impedance Z_{opt} must therefore satisfy

$$Z_{\text{opt}}(\vartheta) = \frac{1 - \mathrm{i}T_0}{D\cos\vartheta + \mathrm{i}T_1}. \tag{18}$$

For the PBE, where the reflection coefficient is given numerically as described in Section 2.2 above, the optimal impedance is found by iteration using a Newton–Raphson method until a sufficiently small reflection coefficient is achieved (for instance, $|R| < 10^{-8}$). As a starting point for the Newton–Raphson iteration, the optimal impedance predicted using the Brambley boundary condition is used as an initial guess; this is found to speed up numerical convergence for each angle of incidence.

4. Results and Discussion

We consider the test cases of the benchmark study proposed by Gabard [5], as listed in Table 1. These parameters are typical of a turbofan aero-engine intake, but are also relevant to other applications: case A is a reference condition; case B represents a thinner boundary layer thickness, such as in the region close to the nacelle intake lip; case C represents the second harmonic of the blade passing frequency; and case D investigates a lower Mach number.

Table 1: Test cases. Taken from Gabard [5].

Case	Helmholtz number, ω	Mach number, M	Boundary layer thickness, δ
A	28	0.55	1.4 %
B	28	0.55	0.7 %
C	56	0.55	1.4 %
D	28	0.30	1.4 %

To access the impact of the boundary layer profile, we consider different analytical formulations. The simpler representation of a sheared flow can be achieved by assuming a linear profile, given by

$$U(y) = \begin{cases} M\dfrac{y}{\delta}, & 0 \le y \le \delta \\ M, & y > \delta. \end{cases} \tag{19}$$

This nonphysical representation gives similar acoustical results when compared to other profiles of the same boundary layer displacement thickness [22], while given its simplicity it is still possible to obtain an explicit solution for all the coefficients of the first and second-order boundary conditions, which can be found in the Appendix A. Two other simple analytic models commonly used to represent the sheared velocity are the parabolic profile

$$U(y) = \begin{cases} M\left(1 - \dfrac{y}{\delta}\right)^2, & 0 \le y \le \delta \\ M, & y > \delta, \end{cases} \tag{20}$$

and the sinusoidal profile

$$U(y) = \begin{cases} M\sin\dfrac{\pi y}{2\delta}, & 0 \le y \le \delta \\ M, & y > \delta, \end{cases} \tag{21}$$

both of which were used by Gabard [5] to access the significance of the boundary layer profile by different boundary conditions. Finally, we also consider the hyperbolic tangent velocity profile,

$$U(y) = \begin{cases} M\tanh\dfrac{y}{\delta_t} & 0 \le y \le \delta \\ M, & y > \delta, \end{cases} \tag{22}$$

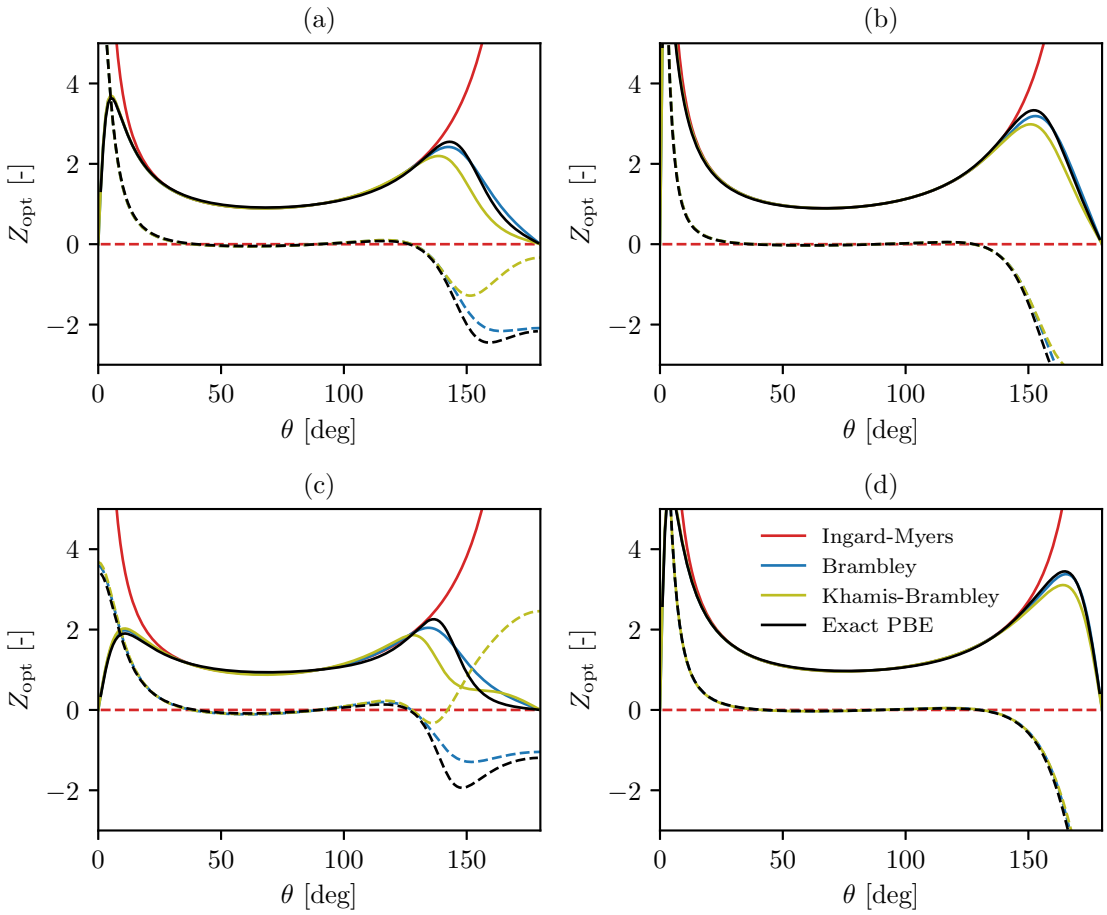

Figure 2: Optimal impedance Z_{opt} in 2D with a linear velocity profile as a function of the angle of incidence θ. Solid lines denote optimal resistances and dashed lines denote optimal reactance. (a) Case A; (b) Case B; (c) Case C; and (d) Case D. (For the coloured version of this figure, the reader is referred to the online version of this article.)

where δ_t is a non-dimensional boundary layer thickness scale which is not the same as the δ above, and which therefore needs to be adjusted for each case [23][2].

4.1. Two-Dimensional Analysis

First, we consider the 2D case shown in Figure 1b and the linear velocity profile. The angle of incidence θ varies from 0° for grazing downstream incidence, to 180° for grazing upstream incidence. For each angle, Figure 2 shows the predicted optimal impedances using the CHE with Ingard–Myers, first order (Brambley), and second order (Khamis–Brambley) boundary conditions, compared to the exact solution obtained using the PBE. The results suggests that the Brambley boundary condition is able to closely follow the exact solution in all cases, except for upstream propagation at high angles of incidence in cases A and C. These conditions are typically found at the turbofan aero-engine intake, which highlights the importance of correctly accounting for boundary layer effects in fan noise propagation. For upstream propagation ($\theta > 90°$), the second order inviscid boundary condition (Khamis–Brambley) leads to higher errors when compared to the first order solution, especially for cases A and C. This finding agrees with Khamis and Brambley [6], who suggest that for thicker boundary layers and higher frequencies the second order terms deviate from the

[2]Using the approximation $\delta_t = \delta/3$ leads to $U(\delta) \approx 0.995M$.

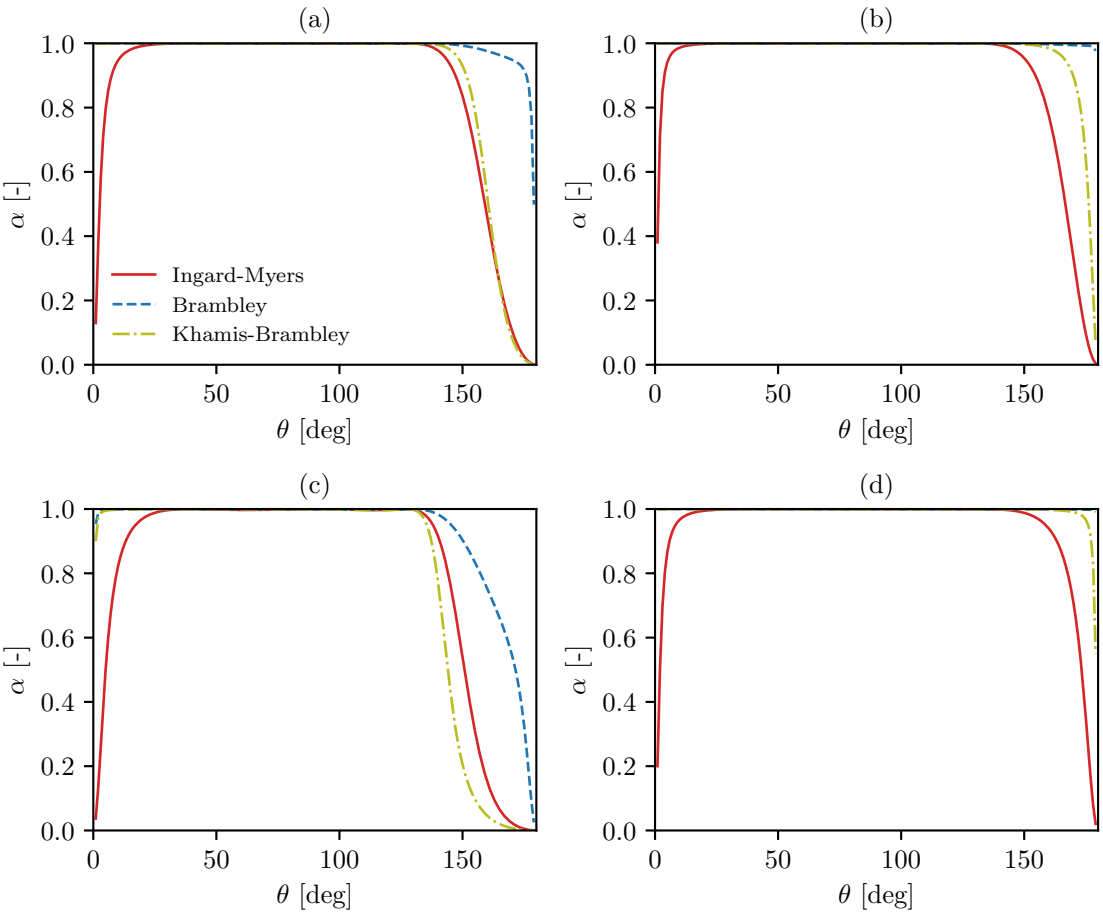

Figure 3: Absorption coefficient α when solving the PBE with optimal impedances predicted by inviscid boundary conditions for the CHE with a linear velocity profile. (a) Case A; (b) Case B; (c) Case C, and; (d) Case D. (For the coloured version of this figure, the reader is referred to the online version of this article.)

exact solution. The optimal impedances of waves propagating at angles near 90° are not affected by the boundary layer, and so all methods give the classic no-flow optimal impedance $Z_{\text{opt}} = 1$.

The optimal resistance predicted by Ingard–Myers boundary condition incorrectly tends to infinity as propagation becomes tangential to the surface, requiring a near-rigid highly-damped wall, a feature also observed in the absence of flow. In contrast, the PBE and the asymptotic boundary conditions predict much lower optimal resistances, which are in line with the results of Spillere and Cordioli [12]. The optimal reactance tends to be positive for downstream propagation and negative for upstream propagation, while the Ingard–Myers boundary condition predicts a zero optimal reactance independent of angle of incidence. For nearly-downstream incidence (with θ close to 0°), the PBE optimum reactance becomes relatively large, although tends to a finite value as $\theta \to 0$, and a similar although less extreme reactance is also seen for nearly-upstream incidence (with θ close to 180°); both of these effects are well captured by the CHE with the Brambley boundary condition.

It is interesting to calculate the absorption coefficient obtained by solving the PBE with the various optimal impedances predicted by either the Ingard–Myers or the asymptotic boundary conditions. The results of this analysis are presented in Figure 3. One may rather look for the reflection coefficient in dB instead of the absorption coefficient. However, for perfect absorption, the absorption coefficient goes to zero and, therefore, the absolute value of the reflection coefficient tends to minus infinity. The reflection coefficient obtained by solving the PBE with the various optimal impedances predicted by either the Ingard–Myers

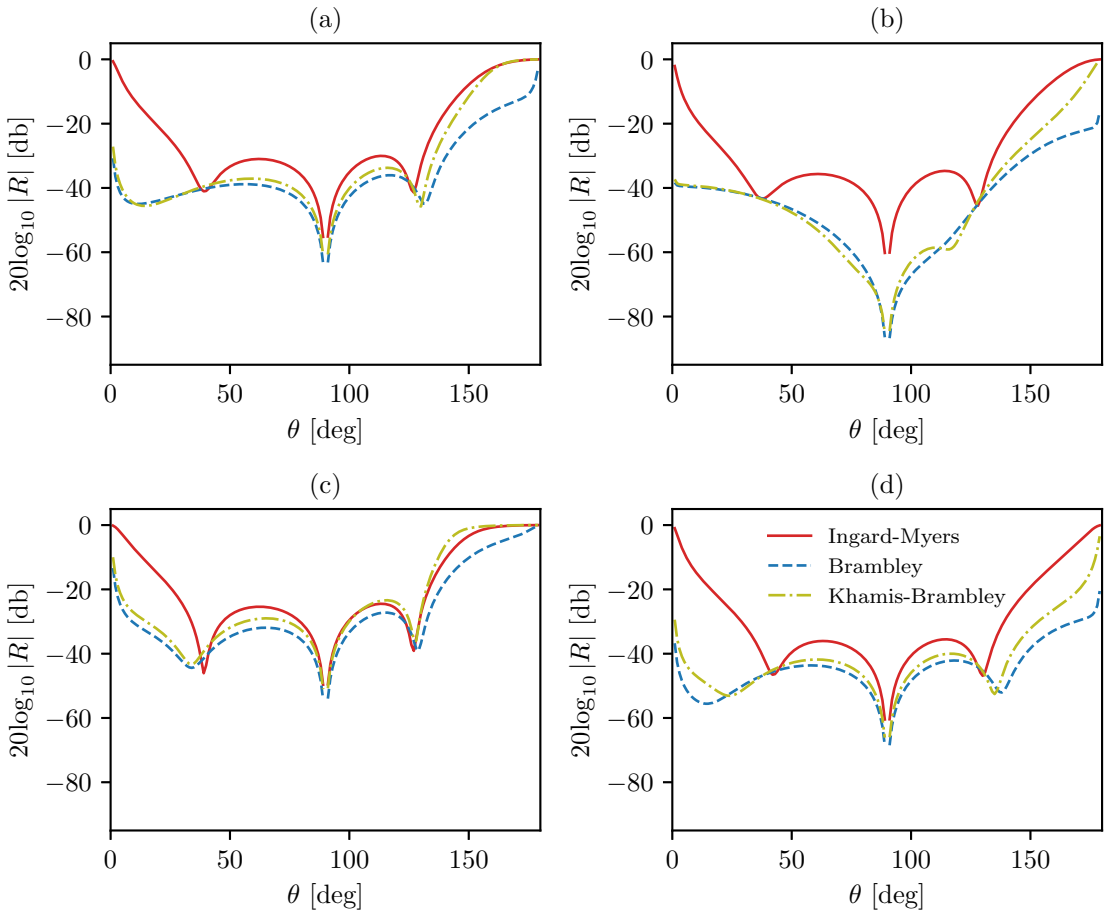

Figure 4: Reflection coefficient $|R|$ on a logarithmic scale when solving the PBE with optimal impedances predicted by inviscid boundary conditions for the CHE with a linear velocity profile. (a) Case A; (b) Case B; (c) Case C, and; (d) Case D. (For the coloured version of this figure, the reader is referred to the online version of this article.)

or the asymptotic boundary conditions are shown in logarithmic scale in Figure 4. Near-perfect absorption is observed for angles between 30° and 130° in all cases, irrespective of the boundary condition used to determine the optimal impedance. However, for acoustic propagation almost parallel to the surface, the Ingard–Myers and the second order asymptotic boundary conditions predict optimal impedances which result in very poor absorption coefficients. This is not surprising, since the predicted impedances by the Ingard–Myers boundary condition tend to infinity as θ approaches 0° or 180°. In other words, the optimal impedance predicted by the Ingard–Myers is, in practice, a hard wall. On the other hand, the optimal impedance predicted by the first order Brambley boundary condition leads to very high absorption, especially in cases B and D, where perfect absorption is achieved at almost all angles of incidence. The same statement is valid for downstream propagation in cases A and C. For upstream propagation, it also represents a considerable improvement over the Ingard–Myers boundary condition.

Next, we consider the effect of the velocity profile shape on the optimal impedance. Initially, all velocity profiles are assumed to have the same boundary layer thickness. For the sake of brevity, we discuss only case A, with the results for the other cases presented in Appendix B. Figures 5a, 5b and 5c show the comparison of the optimal impedance obtained for the parabolic, hyperbolic tangent and sine velocity profiles, respectively, considering the Ingard–Myers, first order and second order asymptotic boundary conditions, compared to the exact solution obtained with the PBE. In Figure 5d, the exact solution obtained for the different velocity profiles are condensed for a clearer comparison. One may notice that the Ingard–Myers

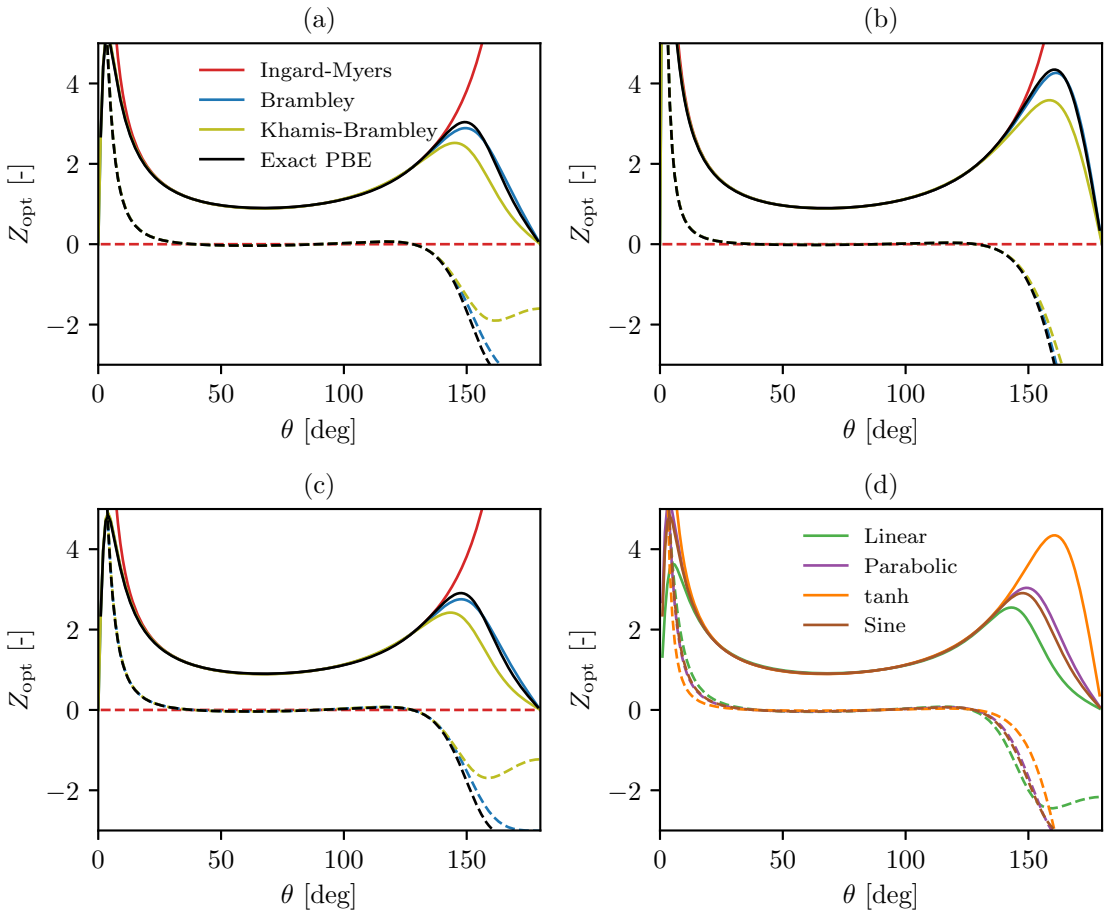

Figure 5: Optimal impedance Z_{opt} for case A in 2D as a function of the angle of incidence θ. Solid lines denote optimal resistances and dashed lines denote optimal reactance. All velocity profiles have the same δ. (a) Parabolic; (b) Hyperbolic tangent; (c) Sinusoidal; and (d) Profiles comparison for the exact solution with PBE. (For the coloured version of this figure, the reader is referred to the online version of this article.)

boundary condition is insensitive to the velocity profile, while the first and second order asymptotic boundary conditions are able to adapt to each of the profiles. As was observed for the linear profile analysis, the optimal impedance predicted by the first order asymptotic boundary condition shows good agreement with the exact solution for the whole range of angles of incidence, for all the considered velocity profiles, especially for the hyperbolic tangent profile. Once again, the second-order boundary condition leads to higher errors when compared to the first order solution, although a better agreement is observed for the hyperbolic tangent profile.

Nayfeh et al. [22] compared the attenuation in bi-dimensional ducts predicted with the Ingard–Myers boundary condition with the exact solution for different velocity profiles. Theirs results suggest that by scaling the velocity profiles for the same **boundary layer displacement thickness**

$$\delta^* = \int_0^\delta 1 - \frac{U(y)}{M} \mathrm{d}y, \tag{23}$$

leads to similar in-duct attenuation. Later, Gabard [5] found that scaling the velocity profiles to have the same boundary layer displacement thicknesses δ^* lead to similar absorption by a flat surface, while matching the boundary layer thicknesses δ lead to mismatches. We now consider the same analysis for the problem of the optimum impedance of a flat surface. The velocity profiles are adjusted such that the parabolic,

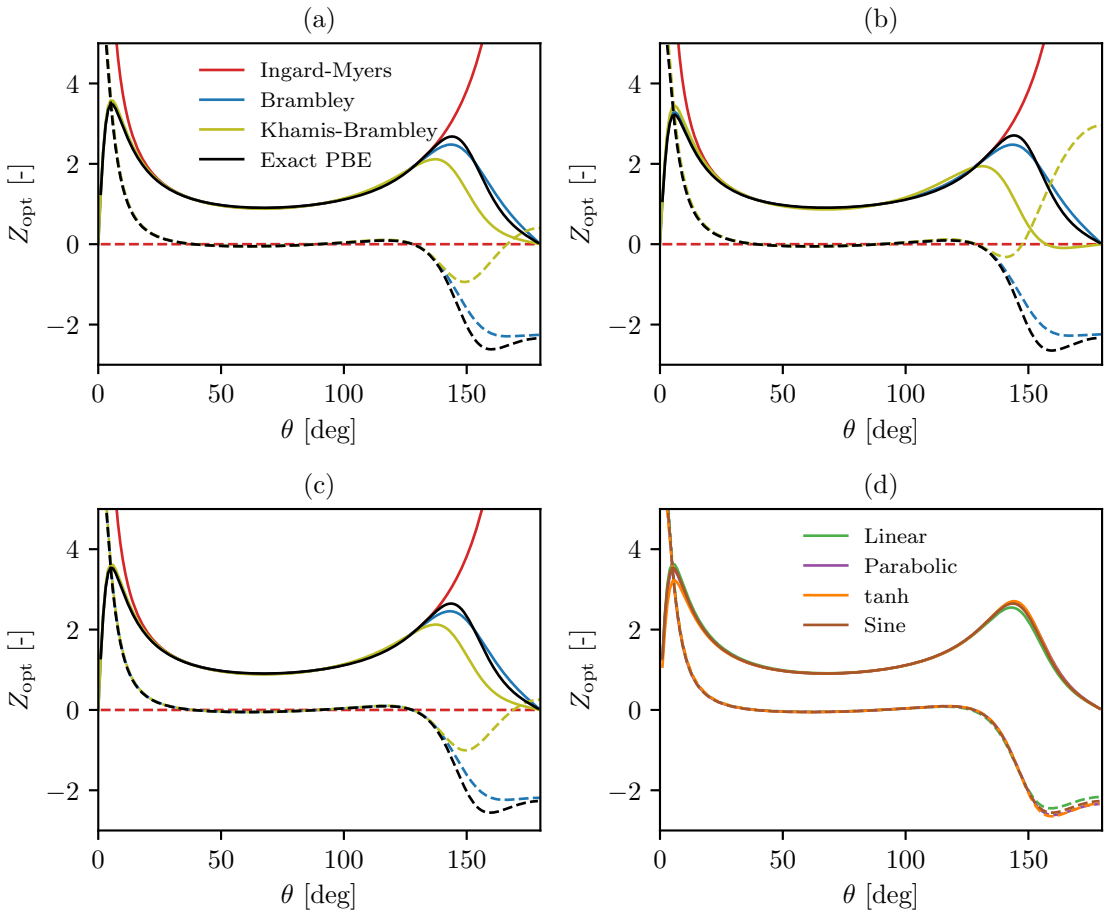

Figure 6: Optimal impedance Z_{opt} for case A in 2D as a function of the angle of incidence θ. Solid lines denote optimal resistances and dashed lines denote optimal reactance. All velocity profiles have the same δ^* for the reference linear profile. (a) Parabolic; (b) Hyperbolic tangent; (c) Sinusoidal; and (d) Profiles comparison for the exact solution with PBE. (For the coloured version of this figure, the reader is referred to the online version of this article.)

hyperbolic tangent and sinusoidal profiles have the same δ_* of the linear profile. Once again we only show the results found for case A, which can be see in Figure 6. An almost perfect agreement is found between the optimal impedance for the different velocity profiles, as can be see in the comparison for the exact solution (Figure 6d). This agrees with the results of the literature [5, 22], since if the same attenuation is expected provided that the boundary layer displacement thickness is kept the same, the optimal impedance therefore should also be kept the same. One may notice that the optimal impedances for the different flow profiles predicted by the first and second order asymptotic boundary conditions are the same, with the only clear exception being the prediction by the second order boundary condition for the hyperbolic tangent velocity profile, for higher angles of upstream incidence. This highlights the hypothesis that the second order asymptotic boundary conditions performs poorly for larger boundary layers, as to achieve a similar δ^* with the hyperbolic tangent flow profile, δ_t needs to be significantly increased.

4.2. Three-Dimensional Analysis

The results from the previous section are now extended to a three-dimensional case, as shown in Figure 1a, where the acoustics waves have angles of incidence ϑ and φ. Figure 7 shows how the predicted optimal resistance and reactance varies for the PBE and the CHE with Ingard–Myers and first order asymptotic boundary conditions. For the sake of conciseness, only results for the test case A are shown, and the second order inviscid boundary conditions is omitted since better agreement was found with the first order

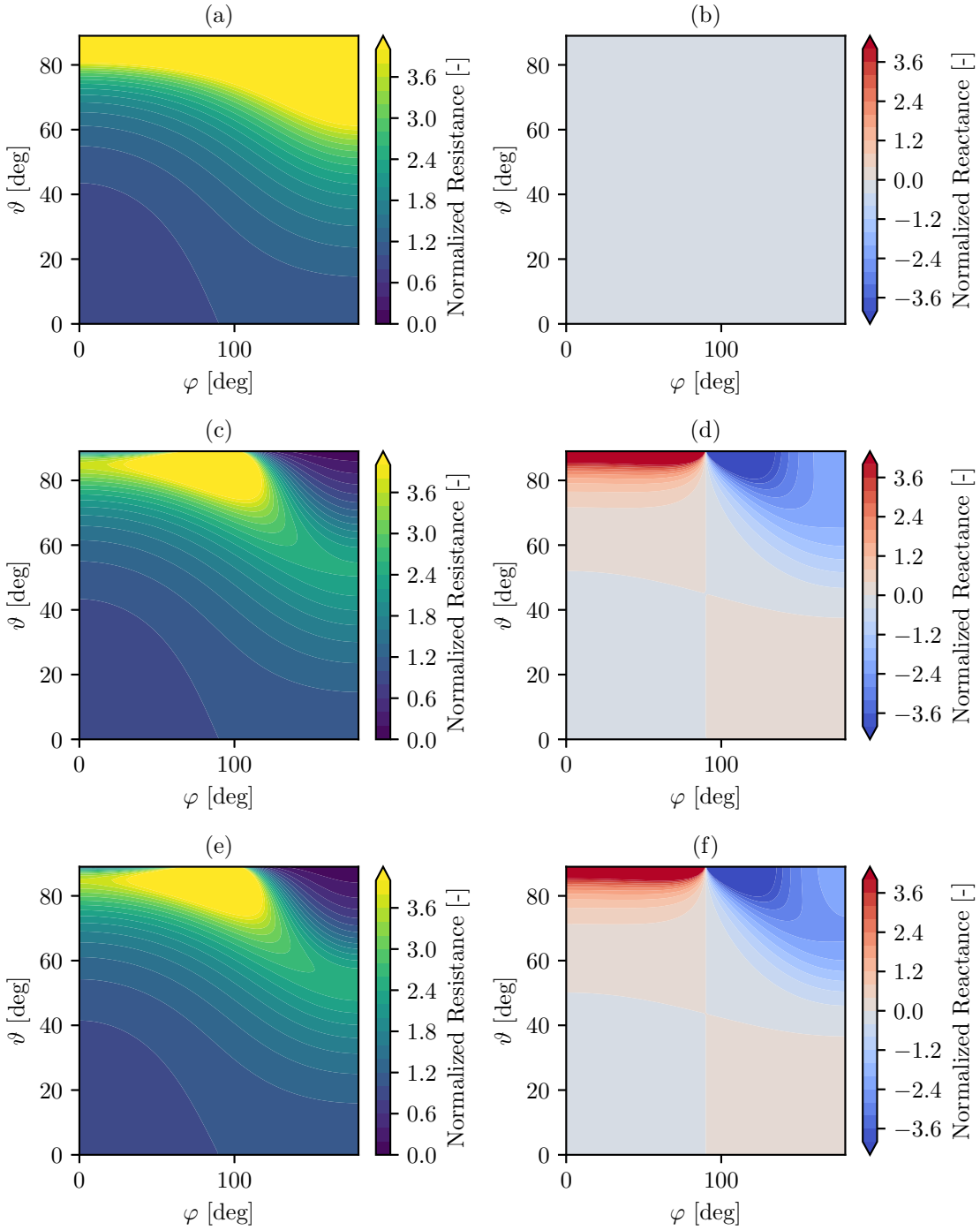

Figure 7: Optimal impedance Z_{opt} for case A as a function of incidence angles ϑ and φ. Optimal resistances (a,c,e) and optimal reactances (b,d,f), considering Ingard–Myers (a,b) and Brambley (c,d) boundary conditions and numerical solution of PBE (e,f). (For the coloured version of this figure, the reader is referred to the online version of this article.)

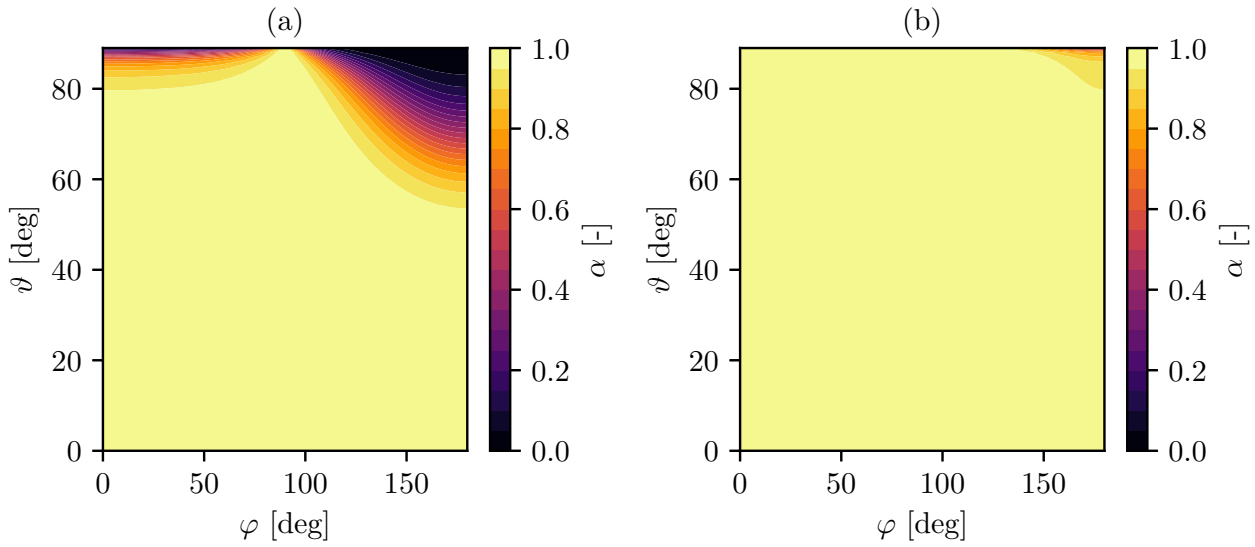

Figure 8: Absorption coefficient α when solving the PBE with optimal impedances predicted by (a) Ingard–Myers and (b) Brambley boundary conditions as a function of incidence angles ϑ and φ. (For the coloured version of this figure, the reader is referred to the online version of this article.)

Brambley boundary condition. Also, only the linear profile is considered here, since similar results observed for the different flow profiles when the same δ^* was considered. Figure 7e shows a complex pattern of optimal impedances for three-dimensional angles of incidence when solving the PBE. As in the 2D case, the Brambley boundary condition is able to capture this pattern (Figure 7c) even at very sharp angles of incidence with ϑ close to 90°, whereas the Ingard–Myers boundary condition fails at these conditions. It should be noted, however, as in the two-dimensional case, at angles close to the normal incidence with ϑ close to 90°, no appreciable difference is observed between the boundary conditions and the reference solution. At $\varphi = 90°$, the acoustic propagation is perpendicular to the flow, and, although no convection is expected, there is still refractive effects, which explains why the optimum impedance is not the classic no-flow optimal impedance. One may also notice the change in the phase of the impedance by the reactances when changing from downstream ($\varphi < 90°$) to upstream ($\varphi > 90°$) propagation. Finally, an important mention is that for normal incidence ($\vartheta = 0°$), all cases predicted the optimal impedance of $Z_{\text{opt}} = 1$, even though it is not clearly noticeable in the surface plots.

As in the two-dimensional case, the error in the absorption coefficient due to the choice of boundary condition is now considered. Figure 8a shows poor absorption for upstream propagation and sharp angles of incidence when using the optimal impedance predicted by Ingard–Myers boundary condition. In the case of downstream propagation, the situation is less dramatic, and reasonable absorption is generally achieved. On the other hand, the Brambley boundary condition (Figure 8b) leads to near perfect absorption at any angle of incidence in the case of downstream propagation. Only at very sharp angles and upstream propagation it is possible to observe some errors, although the absorption coefficients remain relatively high.

5. Conclusions

In this work, the optimal impedance of a lined plane surface in the presence of an inviscid sheared flow was investigated. Different boundary conditions for the convected Helmholtz equation (CHE) were compared to numerical solutions of the Pridmore-Brown equation (PBE). The findings of this work suggests that, for close to normal angles of incidence ($\theta = 90°$, $\vartheta = 0°$), flow effects make minimal difference to the optimal impedance. In this case, the no-flow optimal impedance $Z_{\text{opt}} = 1$ should provide reasonable levels of absorption. When acoustic propagation occurs at more acute angles of incidence, the inclusion of a thin boundary layer becomes crucial to correctly predict the optimal impedance. This effect is more pronounced

for upstream propagation, which represents for instance the case of turbofan aero-engine intake. In general, in both 2D and 3D, excellent agreement is found between the CHE using the Brambley boundary condition and the numerical solution to the PBE in terms of optimal impedance. The Ingard–Myers boundary condition can only be used with satisfactory results at angles close to normal incidence, for which the flow effects are small and the optimal impedance $Z_{\text{opt}} = 1$ is already known.

It is interesting to note that the optimal reactance at acute angles of incidence is significantly nonzero for all but the Ingard–Myers boundary condition. For aeroengine honeycomb liners consisting of an array of Helmholtz resonators, a zero reactance occurs at resonances of the Helmholtz resonators, and this is often thought to be the design point of the liner. Our results here therefore demonstrate that to optimally damp nearly-grazing incidence waves, the liner needs to operate well away from liner resonances, owing to the presence of the flow boundary layer. This effect is missed when using the Ingard–Myers boundary condition.

Different velocity profiles where considered in order to investigate the impact of the profile in the optimal impedance. It was found that the optimal impedance is the same for different velocity profiles if the same boundary layer displacement thickness δ^* is adopted. This is in agreement with previous works that reported similar attenuation for different velocity profiles with the same value of δ^* [5, 22].

An important assumption in this work is the absence of viscothermal effects, which represent the full picture of acoustic propagation in a boundary layer over a lined surface. At conditions similar to turbofan aero-engine intakes, it is known that viscous effects can significantly modify the absorption predictions [24], which could impact the optimal impedance as well. Moreover, in this work the incident acoustic field was assumed to be formed by plane waves. Another possible setup would be assuming a point source over the lined surface. In this configuration, different incidence angles would be observed over the flat surface. Therefore, it is expected that the perfect attenuation may require an impedance distribution, since the optimal impedance depends on the acoustic wave incidence angle.

Acknowledgments

On behalf of L.A. Bonomo, A.M.N Spillere and J.A. Cordioli, this research was partially funded by CNPq (National Council for Scientific and Technological Development). L.A. Bonomo also acknowledges that this study was also financed in part by the Coordenação de Aperfeiçoamento de Pessoal de Nível Superior – Brasil (CAPES), Finance Code 001. E.J. Brambley gratefully acknowledges the support of the UK Engineering and Physical Sciences Research Council (EPSRC grant EP/V002929/1).

Appendix A. Explicit solution of the coefficients in the first and second order boundary conditions for the linear profile

$$\delta I_0 = -\frac{\delta(D-1)(D+2)}{3}, \tag{A.1a}$$

$$\delta I_1 = \frac{\delta(D-1)}{D}, \tag{A.1b}$$

$$\delta^2 I_2 = -\delta^2\left(\frac{(D-1)(D+3)}{12}\right), \tag{A.1c}$$

$$\delta^2 I_3 = \delta^2\left(\frac{(D-1)(D-3)+2\log D}{2(D-1)^2}\right), \tag{A.1d}$$

$$\delta^2 I_{01} = \delta^2\left(\frac{(1-D)(1+D^2)((D-1)(D+2)-6)-12D\log D}{12D(D-1)^2}\right), \tag{A.1e}$$

$$\delta^2 I_{10} = -\delta^2\left(\frac{(D-1)(12+(D-1)((D-1)(3D+1)-6))-12\log D}{12(D-1)^2}\right), \tag{A.1f}$$

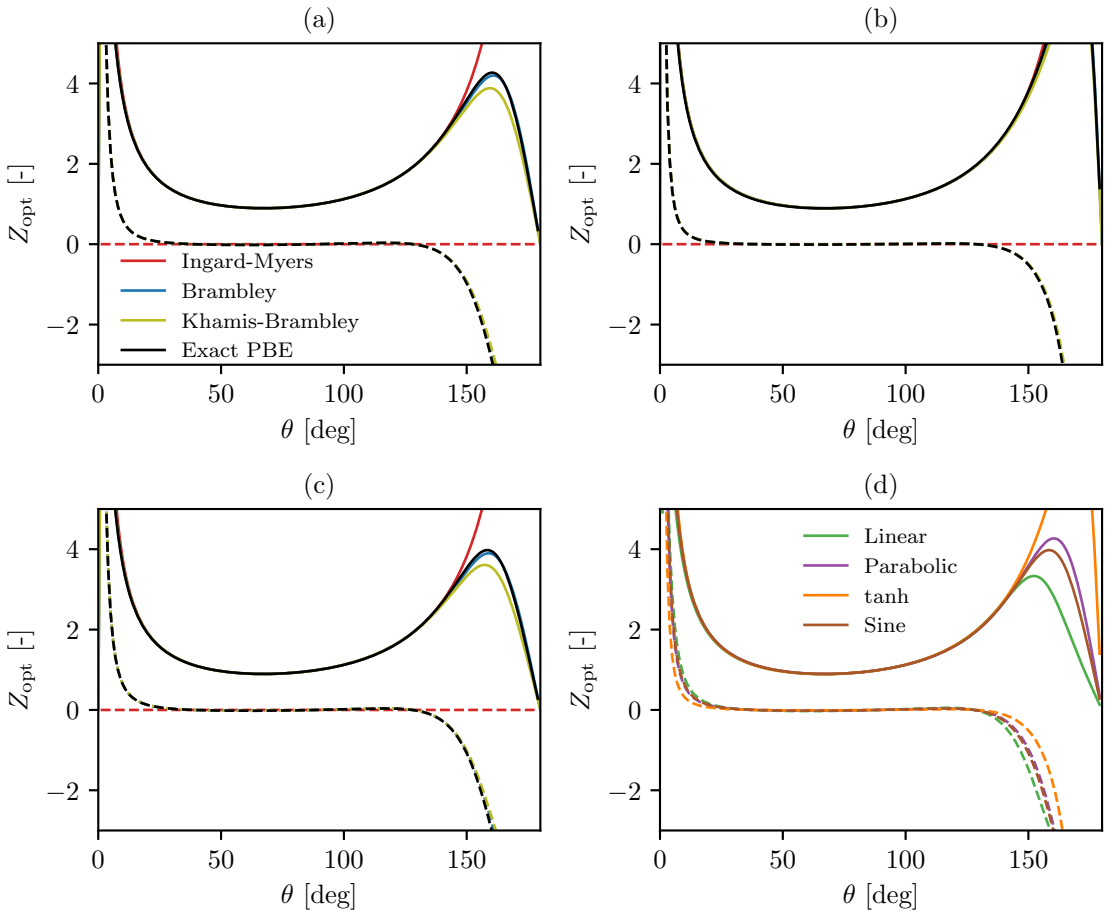

Figure B.9: Optimal impedance Z_{opt} for case B in 2D as a function of the angle of incidence θ. Solid lines denote optimal resistances and dashed lines denote optimal reactance. (a) Parabolic; (b) Hyperbolic tangent; (c) Sinusoidal; and (d) Profiles comparison. (For the coloured version of this figure, the reader is referred to the online version of this article.)

$$\delta^2 I_{00} = \delta^2 \left(\frac{(D-1)(2\delta(D+2) - 3(D-1) - 8)}{12} \right), \tag{A.1g}$$

and

$$\delta^2 I_{11} = \frac{\delta}{2D} \left(\frac{\delta + \delta(1-\delta)(D-1) + 2\delta D - 1 - D\log D}{(D-1)^2} \right). \tag{A.1h}$$

Appendix B. Optimal impedances in 2D for different velocity profiles

Figures B.9, B.10 and B.11 plot the same comparison as figure 5 but for Cases B, C and D respectively.

References

[1] E. J. Brambley, Well-posed boundary condition for acoustic liners in straight ducts with flow, AIAA Journal 49 (2011) 1272–1282. doi:10.2514/1.j050723.

[2] W. Eversman, R. J. Beckemeyer, Transmission of Sound in Ducts with Thin Shear Layers—Convergence to the Uniform Flow Case, The Journal of the Acoustical Society of America 52 (1972) 216–220. doi:10.1121/1.1913082.

[3] U. Ingard, Influence of fluid motion past a plane boundary on sound reflection, absorption, and transmission, The Journal of the Acoustical Society of America 31 (1959) 1035–1036. doi:10.1121/1.1907805.

[4] M. K. Myers, On the acoustic boundary condition in the presence of flow, Journal of Sound and Vibration 71 (1980) 429–434. doi:10.1016/0022-460X(80)90424-1.

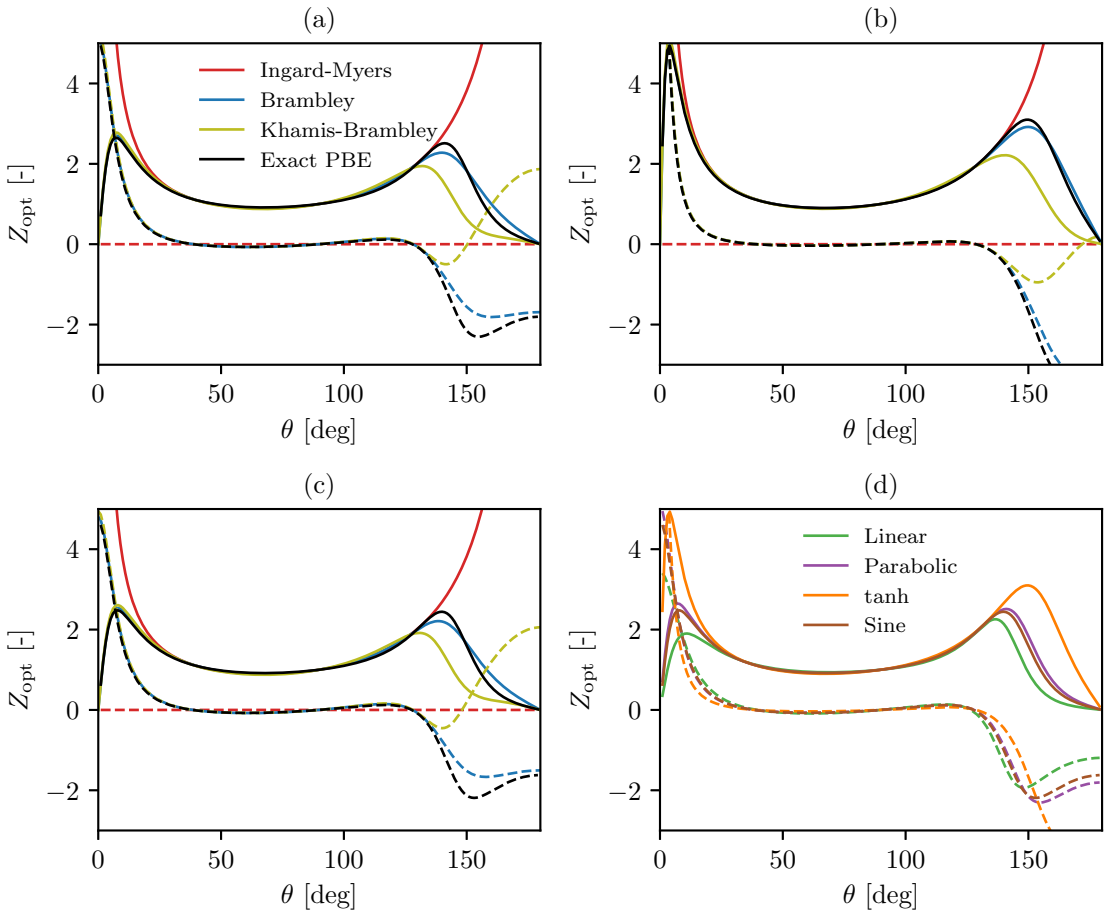

Figure B.10: Optimal impedance Z_{opt} for case C in 2D as a function of the angle of incidence θ. Solid lines denote optimal resistances and dashed lines denote optimal reactance. (a) Parabolic; (b) Hyperbolic tangent; (c) Sinusoidal; and (d) Profiles comparison. (For the coloured version of this figure, the reader is referred to the online version of this article.)

[5] G. Gabard, A comparison of impedance boundary conditions for flow acoustics, Journal of Sound and Vibration 332 (2013) 714–724. doi:10.1016/j.jsv.2012.10.014.

[6] D. Khamis, E. J. Brambley, Acoustic boundary conditions at an impedance lining in inviscid shear flow, Journal of Fluid Mechanics 796 (2016) 386–416. doi:10.1017/jfm.2016.273.

[7] A. Färm, S. Boij, R. Glav, O. Dazel, Absorption of sound at a surface exposed to flow and temperature gradients, Applied Acoustics 110 (2016) 33–42. doi:10.1016/j.apacoust.2016.03.017.

[8] L. Cremer, Theory regarding the attenuation of sound transmitted by air in a rectangular duct with an absorbing wall, and the maximum attenuation constant produced during this process, Acustica 3 (1953) 249–263. In German.

[9] J. Schauer, E. Hoffman, Optimum duct wall impedance-shear sensitivity, in: 13th Aerospace Sciences Meeting, Pasadena, CA, USA, 1975.

[10] B. Tester, The propagation and attenuation of sound in lined ducts containing uniform or "plug" flow, Journal of Sound and Vibration 28 (1973) 151–203. doi:10.1016/S0022-460X(73)80102-6.

[11] Z. Zhang, H. Bodén, M. Åbom, The cremer impedance: An investigation of the low frequency behavior, Journal of Sound and Vibration 459 (2019) 114844. doi:10.1016/j.jsv.2019.07.010.

[12] A. M. N. Spillere, J. A. Cordioli, Optimum acoustic impedance in circular ducts with inviscid sheared flow: Application to turbofan engine intake, Journal of Sound and Vibration 443 (2019) 502–519. doi:10.1016/j.jsv.2018.12.007.

[13] A. Cavalieri, W. Wolf, J. Jaworski, Numerical solution of acoustic scattering by finite perforated elastic plates, Proceedings of the Royal Society A: Mathematical, Physical and Engineering Sciences 472 (2016) 20150767. doi:10.1098/rspa.2015.0767.

[14] C. Pimenta, W. Wolf, A. V. Cavalieri, Acoustic scattering by 3d poroelastic plates with swept trailing edges, in: 23rd AIAA/CEAS Aeroacoustics Conference, Denver, Colorado, USA, 2017, pp. 1–21.

[15] L. Rego, F. Avallone, D. Ragni, D. Casalino, H. Denayer, Acoustic liners for jet-installation noise reduction, Journal of Sound and Vibration 537 (2022) 117189. doi:10.1016/j.jsv.2022.117189.

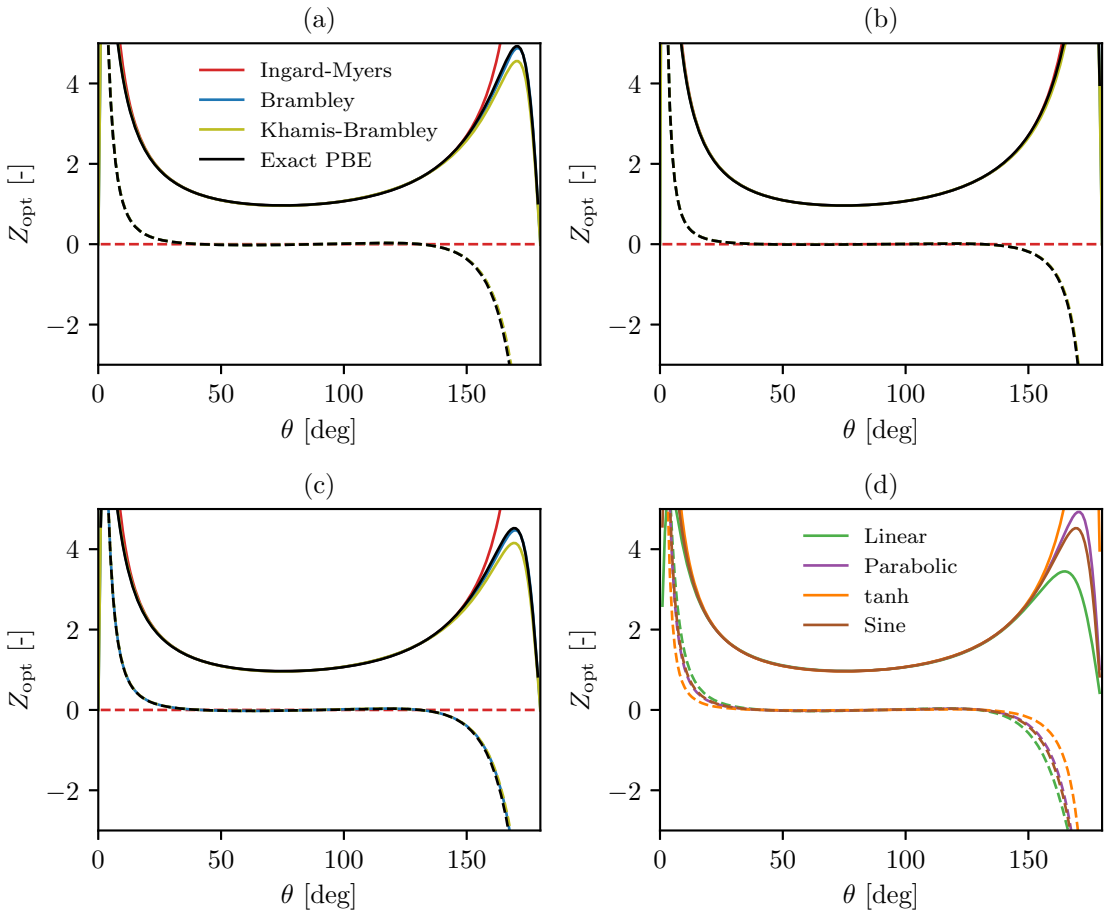

Figure B.11: Optimal impedance Z_{opt} for case D in 2D as a function of the angle of incidence θ. Solid lines denote optimal resistances and dashed lines denote optimal reactance. (a) Parabolic; (b) Hyperbolic tangent; (c) Sinusoidal; and (d) Profiles comparison. (For the coloured version of this figure, the reader is referred to the online version of this article.)

[16] J. R. Sirotto, L. A. Bonomo, J. A. Cordioli, On the application of acoustic liners for the reduction of jet-flap installation noise, Applied Acoustics 221 (2024) 110029. doi:/10.1016/j.apacoust.2024.110029.

[17] D. C. Pridmore-Brown, Sound propagation in a fluid flowing through an attenuating duct, Journal of Fluid Mechanics 4 (1958) 393–406. doi:10.1017/S0022112058000537.

[18] P. Morse, U. Ingard, Theoretical Acoustics, 1 ed., Princeton University Press, Princeton, New Jersey, USA, 1986.

[19] D. Khamis, E. J. Brambley, Viscous effects on the attenuation of a plane wave by an acoustic lining in shear flow, The Journal of the Acoustical Society of America 141 (2017) 2408–2417. doi:10.1121/1.4979469.

[20] J. Boyd, Chebyshev and Fourier Spectral Methods, Dover Books on Mathematics, 2 ed., Dover Publications, Mineola, NY, USA, 2001.

[21] E. Anderson, Z. Bai, C. Bischof, L. Blackford, J. Demmel, J. Dongarra, J. Du Croz, A. Greenbaum, S. Hammarling, A. McKenney, D. Sorensen, LAPACK Users' Guide, 3 ed., Society for Industrial and Applied Mathematics, Philadelphia, PA, USA, 1999.

[22] A. H. Nayfeh, J. E. Kaiser, B. S. Shaker, Effect of mean-velocity profile shapes on sound transmission through two-dimensional ducts, Journal of Sound and Vibration 34 (1974) 413–423. doi:10.1016/S0022-460X(74)80320-2.

[23] S. Rienstra, G. Vilenski, Spatial instability of boundary layer along impedance wall, in: 14th AIAA/CEAS Aeroacoustics Conference (29th AIAA Aeroacoustics Conference), Vancouver, British Columbia, Canada, 2008, pp. 1–13.

[24] D. Khamis, E. J. Brambley, Viscous effects on the acoustics and stability of a shear layer over an impedance wall, Journal of Fluid Mechanics 810 (2017) 489–534. doi:10.1017/jfm.2016.737.